

SOL-GEL SYNTHESIS, CHARACTERIZATION AND IN VITRO EVALUATION OF SiO₂-CaO-P₂O₅ BIOACTIVE GLASS NANOPARTICLES WITH VARIOUS CaO/P₂O₅ RATIOS

S. M. AHMADI^a, A. BEHNAMGHADER^{b*}, A. ASEFNEJAAD^a

^a*Department of Biomedical Engineering, Science and Research Branch, Islamic Azad University, Tehran, Iran*

^b*Biomaterials Group, Department of Nanotechnology and Advanced Materials, Materials & Energy Research Center, Karaj, Iran*

Bioactive glass nanoparticles in ternary system of SiO₂-CaO-P₂O₅ with various CaO/P₂O₅ molar ratios of 4.75, 9.5, and 19 were synthesized via sol-gel method using TEOS, TEP and calcium nitrate precursors. Characterization of the synthesized bioactive glass powders by the way of XRD, FTIR, FESEM, and EDS techniques revealed the formation of amorphous glasses with high elemental purity. The sample with CaO/P₂O₅ equal to 9.5, revealed the best biomineralization through immersion in SBF. According to the results of biodegradation trials in citric acid solution, the glass samples with higher CaO/P₂O₅ presented more considerable weight loss and variations in elemental concentration. As a result of apatite layer formation in SBF, weight loss and elemental release/depletion showed less sensitive to the CaO/P₂O₅ molar ratio. The cytotoxicity of bioactive glass was evaluated using MTT test by seeding the osteosarcoma cells (G292) on powder for different days. MTT results showed the non-toxicity of the synthesized bioactive glass nanoparticles.

(Received May 25, 2017; Accepted August 21, 2017)

Keywords: Bioactive glass; SiO₂-CaO-P₂O₅; Nanoparticles; Sol-gel synthesis; In Vitro Study

1. Introduction

Regeneration of bone tissue damages resulted from traumatism, infectious processes, neoplasms and congenital malformations is a field of focus in biomedicine [1- 4]. Bone grafts, including autografts, allografts, xenografts and artificial grafts are extensively employed in clinical applications for replacement and repair of bone tissues in defect sites [3, 5, 6]. There is a great tendency for development of bioactive materials with engineered structures to be used in artificial bone grafts providing the support for the body to manage the reconstruction [4, 7]. Indeed, the goal is to stimulate the regeneration of the damaged tissues by the human body. To this end, various biomaterials such as carbonates [8], calcium phosphates [9], aluminosilicates (geopolymers) [10], and bioactive glasses [11-13] have been developed and employed. Among them, bioactive glasses have shown to be a satisfying candidate due to their superior bioactivity, osteoconductivity and osteoproductivity which confer them the ability to repair and replace the diseased or damaged bone [14, 15]. These properties are resulted from their progressive dissolution in physiological medium, where the release of calcium, phosphate, and sodium ions could stimulate the growth of a biocompatible apatite layer forming a strong bond with the surrounding bone tissues [14, 16, 17].

Since the discovery of the first generation of bioactive glass compositions, 45S5 Bioglass[®] (45% SiO₂, 24.5% CaO, 24.5% Na₂O and 6% P₂O₅ (wt.%)), by Hench et al. in 1969 [18], various bioactive glasses have been developed for biomedical applications [4, 19]. 58S bioactive glass has received special attention as scaffold material owing to its excellent bioactivity, good

*Corresponding author: behnamghader@yahoo.com

biodegradability, and bone-bonding ability [13, 20]. 58S bioactive glass can react with physiological fluids to form direct bonds with bone tissue in the early time of implantation without any toxicity, inflammation and foreign-body response [21-23].

Bioactive glasses can be produced by melting method at ~ 1350 °C or sol-gel method at lower calcination temperature [12-14]. There are several advantages of a sol-gel derived glass over a melt-derived glass which are determinant factors for making bioactive materials employed in tissue engineering [11]. Some of these merits include lower processing temperature, higher range of SiO₂ usage (up to 90 mol%), lack of necessity of sodium oxide (which is used in conventional melt-derived bioactive glasses), and final glass product with higher bioactivity and nano-scale porosity making the bioactive glass desirable to be impregnated with biologically active agents such as growth factors [22, 24]. The lower heating temperature in sol-gel method results in increased numbers of silanol groups or mesopores acting as nucleation sites for apatite formation in the bioactive glasses [11]. In this way the bioactivity process has been investigated both *in vitro* during interactions between bioactive glasses and biological fluids and *in vivo* during interactions with bony tissues. The process includes a complex series of physico-chemical reactions such as dissolution, diffusion, ionic exchange and precipitation [25]. The sequence of events leading to formation of bioactive apatite layer includes ion release from the bioactive glass, formation of silanol groups (Si-OH) on surface of the glass, adsorption of calcium and phosphate ions on the glass surface stimulating the nucleation of amorphous calcium phosphate nanoclusters, and eventually growth and crystallization of the calcium phosphate (apatite) layer [25, 26].

Up to now, a few reports have been published on effect of CaO/P₂O₅ ratio on properties of SiO₂-CaO-P₂O₅ bioactive glasses synthesized via sol-gel method. Salinas et al. synthesized three gel glasses containing 25 mol% of CaO and SiO₂ + P₂O₅ content of 75 + 0, 72.5 + 2.5, and 70 + 5 mol%. The effect of glass composition on textural properties (surface area and porosity) and *in vitro* behavior of bioactive glasses has been investigated. The results confirmed that upon increase of P₂O₅ content, the surface area increases, the pore volume decreases and the crystallization of bioactive apatite layer was found after shorter periods in SBF [27]. Padilla et al. synthesized bioactive glasses with compositions 70SiO₂-30CaO and 70SiO₂-26CaO-4 P₂O₅ (mol%) using sol-gel method. According to the obtained results, the presence of phosphorus in the raw glasses induces the glass crystallization, easier formation of bioactive layer and heterogeneous distribution of defects in the glasses worsening their mechanical properties [28]. Zhao et al. synthesized mesoporous bioactive glasses containing different P₂O₅ molar percentages of 10, 20, and 30 using sol-gel method. The results showed that the glasses with high P₂O₅ content have more orthophosphate groups in isolated crystalline nano-regions leading to better bioactivity during the SBF immersion. Also, more apparent and denser plate-like apatites were formed on glasses with higher P₂O₅ content [29].

In this study, bioglass nanoparticles in ternary system of SiO₂-CaO-P₂O₅ with various compositions were synthesized using the sol-gel method. Various CaO/P₂O₅ molar ratios of 4.75 (BG-L), 9.50 (BG-M), and 19.00 (BG-H) were studied. The microstructure and chemical composition of the glasses were investigated by scanning electron microscopy/energy dispersive spectroscopy (SEM/EDS), Fourier transform infrared spectroscopy (FTIR), X-ray diffraction (XRD) and field emission transmission electron microscopy (FE-TEM). *In vitro* biomineralization, biodegradation and biocompatibility of as-synthesized bioactive glasses in simulated body fluid (SBF) and citric acid solution (pH 3.0) at 37 °C were studied using FTIR, SEM-EDS, ICP-AES and MTT cytotoxicity assay.

2. Materials and method

2.1. Materials

All materials used in the experiments were of analytical grade and purchased from Sigma Aldrich.

2.2. Synthesis of bioactive glass nanoparticles

Three types of bioactive glasses were synthesized according to the compositions summarized in Table 1. To synthesize the bioglass nanoparticles via sol-gel method, firstly tetraethyl orthosilicate (TEOS) precursor was dissolved in 1.0 M nitric acid (HNO₃) under stirring condition. In the following, triethyl phosphite (TEP) and Ca(NO₃)₂·4H₂O (CaN) precursors were sequentially added to the solution. The resulting transparent sol was kept at room temperature for 5 days to transform into gel through polycondensation reactions. The as-formed gel was hold in oven at 60 °C for 2 days to complete condensation over time and further dried at 120 °C for 2 days. The powders were calcined at 650 °C for 2 h and finally were ground using a planetary ball-mill at 300 rpm for 3 h.

Table 1 Chemical composition and the amount of precursors consumed for synthesis of bioactive glass nanoparticles

Precursors	Bioactive glasses		
	BG-L	BG-M	BG-H
TEOS (% mol.)	58.0	58.0	58.0
TEP (% mol.)	7.3	4.0	2.1
CaN (% mol.)	34.7	38.0	39.9
CaO/P ₂ O ₅ molar ratio	4.75	9.50	19.00

2.3. Characterization of bioactive glass nanoparticles

To investigate the thermal behavior of the bioglass powders and to design an efficient heat treatment for the subsequent stabilization, simultaneous thermogravimetry and differential thermal analysis (TG-DTA, PL-STA 1600) was performed on the dried gels from room temperature to 1000 °C under atmospheric condition with a heating rate of 10 °C/min.

The phase analysis of bioactive glass powders was conducted on a Philips-pw 3710 X-ray diffractometer (XRD) equipped with a Cu-K α ($\lambda = 1.542 \text{ \AA}$) rotating anode operated at 40 kV and 30 mA. The patterns were collected over an angular range of 20° to 70°, with 0.02° step-size and scan speed of 2°/min.

The functional groups of the bioglass powders were analyzed by Fourier transfer infrared (FTIR) spectroscopy performed on a Thermo Nicolet spectrophotometer over the wavenumber range of 400–4,000 cm⁻¹.

The microstructure and morphology of the samples were studied by field-emission scanning electron microscopy (FESEM-Tescan, Czech Republic) with accelerating voltage of 15 kV.

2.4. In vitro bioactivity study

In vitro bioactivity experiments were performed by soaking 10 mg of bioglass powders in 10 ml of simulated body fluid (SBF) and citric acid solution (pH 3.0) at 37 °C in sterile polyethylene containers for time periods from 1 to 14 days. After rinsing with deionized water and drying in air at room temperature, the samples were characterized by SEM (AIS2300C, Seron Technologies), FTIR and Raman spectrometer (Senterra, Bruker) equipped with high-energy laser diodes at the wavelength of 785 nm. During the tests, the variation of pH and the weight of immersed powders were measured. Furthermore, the concentration of released ions (phosphorus (P), silicon (Si) and calcium (Ca)) in SBF and citric acid were measured at different time periods using inductively coupled plasma atomic emission spectroscopy (ICP-OES, Optima 8000). In each case, three repetitive samples were analyzed to determine the standard error and significance of differences.

The chemical composition and elemental purity of the bioglass powders and biomimetic precipitates were evaluated by energy dispersive X-ray spectroscopy (EDS).

The cytotoxicity of the synthesized bioactive glass nanoparticles was examined by colorimetric MTT (3-(4,5-dimethylthiazol-2-yl)-2,5-diphenyltetrazolium bromide) tetrazolium reduction assay. To this purpose, the human osteoblast (G-292) cells were used. The samples were

washed under ultrasonification with sterile distilled water. After disinfecting under ultraviolet light, the samples were kept in sterilized appropriate flasks. Cells were seeded in a 96-well plate (cell density of 1.5×10^4 cell/mL) containing RPMI culture medium with 10% FBS and 1% Pen Strep antibiotic which was loaded by 500 μg of bioactive glass nanoparticles (sterilized by ethanol (70 wt.%), UV radiation for 20 min and autoclaving at 120 $^{\circ}\text{C}$ for 30 min). The plates were kept in incubator at 37 $^{\circ}\text{C}$, 98% RH, and 5% CO_2 for 24 h. After incubation, the medium was exchanged with 100 μL of conditioned culture medium containing 10% MTT solution and kept for 4 h. Then, culture medium was removed and 100 μL of dimethyl sulfoxide (DMSO) was added to dissolve the resulting formazan. The optical absorbance of the resulted blue-violet solution was measured by ELISA microplate reader (Sunrise-Tecan, Austria) at $\lambda=570$ nm. The results were reported as the mean \pm standard deviation (SD) from triplicate wells. Differences were considered statistically significant at $p < 0.05$.

3. Results and discussion

3.1. Characterization of bioactive glass powders

Fig. 1 shows the TG/DTA curves of as-dried gels before stabilization. TG curves can be divided into three zones. The amount of weight loss at any stage is shown in Table 2. An endothermic peak at temperature range of 70-200 $^{\circ}\text{C}$ can be assigned to the water/moisture removal and loss of pore liquor in the gels [11, 13]. In the range of 200-500 $^{\circ}\text{C}$, several endothermic and some exothermic reactions can be attributed to thermal degradation of organic residues and beginning of nitrate decomposition reaction. This decomposition is a stepwise reaction that thermodynamically takes place at temperatures below 550 $^{\circ}\text{C}$ [8, 12]. The thermal decomposition of nitrates and silanol groups happen at temperatures ranging from 400-600 $^{\circ}\text{C}$ (mostly between 530-600 $^{\circ}\text{C}$). The exothermic peak observed at about 850 $^{\circ}\text{C}$ indicates the crystallization of bioglass [11-13, 20]. No significant weight loss is observed above ~ 700 $^{\circ}\text{C}$ suggesting the completion of elimination reactions and fully removal of residues.

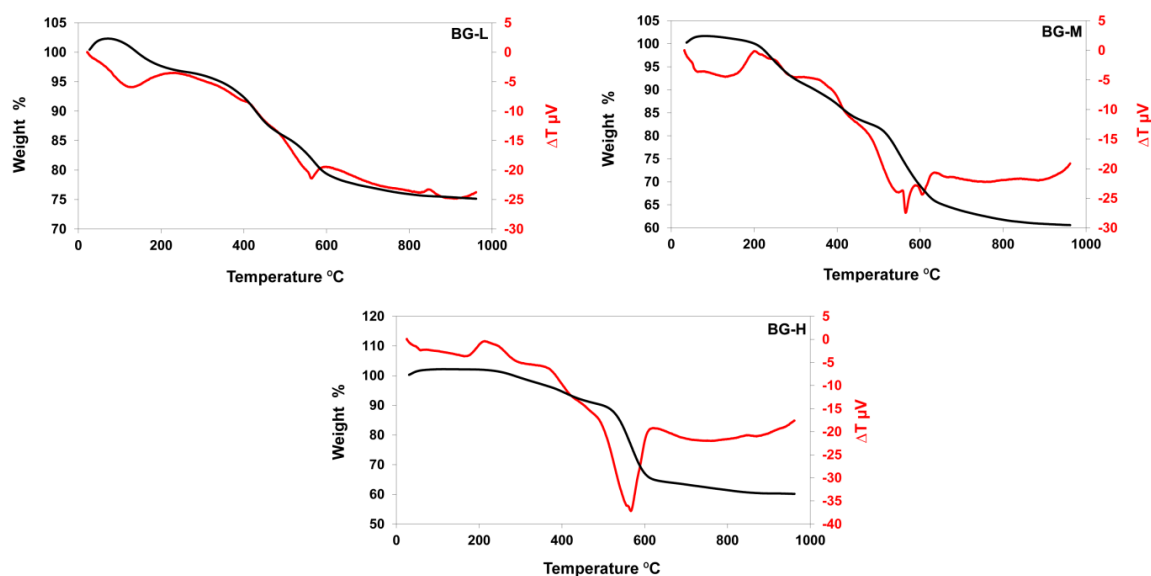


Fig. 1 TG/DTA curves for as-dried gels.

Table 2 Amount of weight loss in the dried gels

Sample	Weight loss (% wt.)		
	70-200 °C	200-500°C	530-600 °C
BG-L	4.0	17.0	4.0
BG-M	3.0	30.0	5.0
BG-H	1.0	36.0	3.0

Fig. 2 shows the XRD patterns of BG-L, BG-M and BG-H bioactive glass powders heat treated at 650 °C. The figure revealed broad diffraction characteristics of amorphous glass. There also can be found some peaks with very low intensity related to crystalline phases including CaSiO_3 (JCPDS 42-0547) and pseudowollastonite $\text{Ca}_3(\text{Si}_3\text{O}_9)$ (JCPDS 74-0874) [13, 19]. The absence of diffractions related to nitrate compounds and other impurities suggests the high purity of the synthesized glass nanoparticles.

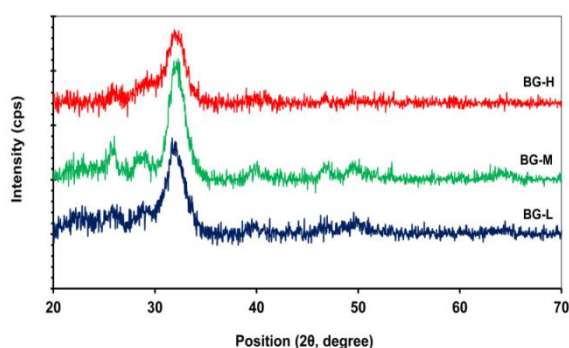


Fig. 2. XRD patterns of the synthesized bioactive glass powders heat treated at 650 °C.

FTIR spectra of BG-L, BG-M and BG-H bioactive glass powders after heat treatment at 650 °C are shown in Fig. 3. The absorption bands centered at $\sim 464 \text{ cm}^{-1}$ and $\sim 810 \text{ cm}^{-1}$ are characteristic of the silicate network and respectively ascribed to the Si-O-Si symmetric bending and Si-O symmetric stretching of bridging oxygen atoms between tetrahedrons. The strong absorption band in the region $900\text{--}1200 \text{ cm}^{-1}$ is assigned to Si-O-Si stretching and/or P-O stretching vibrations in the glass network. The peaks located at ~ 865 , ~ 1432 and $\sim 1461 \text{ cm}^{-1}$ are due to the presence of carbonate (CO_3^{2-}). The small peak emerged at wavenumber of $\sim 920 \text{ cm}^{-1}$ is related to the Si-O-Ca groups. It can be seen that the intensity of the aforementioned peak increases by increase of the CaO/P₂O₅ ratio. The broad peak centered at around 3460 cm^{-1} and a peak at 1635 cm^{-1} are assigned to the stretching and bending vibrations of O-H group in adsorbed water molecules [5, 23, 30]. There cannot be found any trace of nitrate functional groups in the spectra. The FTIR results are in good agreement with the XRD results revealing the high purity of the synthesized glass nanoparticles.

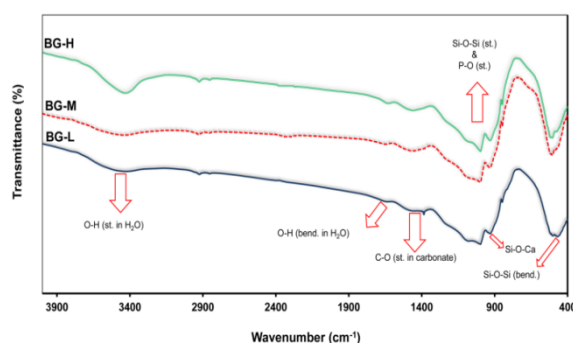


Fig. 3. FTIR spectra the synthesized bioactive glass powders heat treated at 650 °C

Fig. 4 shows FESEM micrographs of bioactive glass powders after heat treatment at 650 °C. The micrographs clearly show the ground powder constitutes aggregates which are composed of spherical nanoparticles ranging from 40 to 60 nm. It seems that the size and morphology of glass powders do not undergo significant changes with changing composition. The EDS patterns shown as insets in Fig. 4 display the elemental composition of the synthesized bioactive glass nanoparticles. The patterns clearly show that all bioactive glasses are only composed of Ca, Si, O, and P elements. Some traces of Au elements in the patterns are resulted from coating samples with gold. The absence of other elements in the synthesized bioglass nanoparticles represents their high elemental purity.

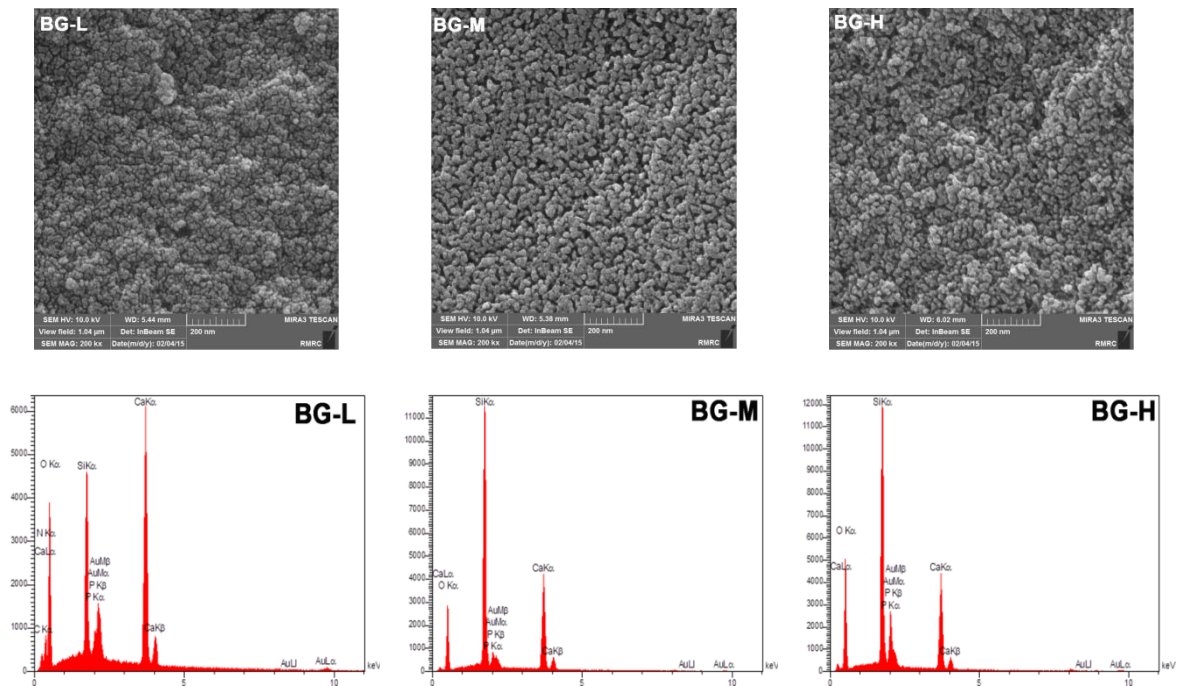


Fig. 4 FESEM micrographs and EDS patterns of BG-L, BG-M and BG-H bioactive glass powders heat treated at 650 °C

3.2. In vitro studies

In order to evaluate the cellular *in vitro* behavior and degradation of bioglass samples in SBF and citric acid, chemical and elemental analysis, morphological characteristics, pH variations, and amount of weight loss were examined.

FTIR spectra of bioactive glass powders after soaking both in SBF and citric acid are shown in Fig. 5. According to the spectra, upon soaking in SBF for various times from 1 to 14 days, the twin bands characteristics of apatite deposits positioned at 570 cm^{-1} and 602 cm^{-1} (asymmetric vibrations of P-O band) gradually begin to appear. In addition, the soaked glasses in SBF show the broad absorption band centered at 1440 cm^{-1} and sharp vibrational peak at $\sim 900 \text{ cm}^{-1}$ assigning to the stretching mode of carbonate (CO_3^{2-}) groups. These findings confirm the formation of carbonated apatite on surface of the nanoparticles upon soaking in SBF suggesting the good bioactivity of the as-prepared bioglass powders. However, the samples immersed in the citric acid do not exhibit any sign of apatite formation [22, 29, 30].

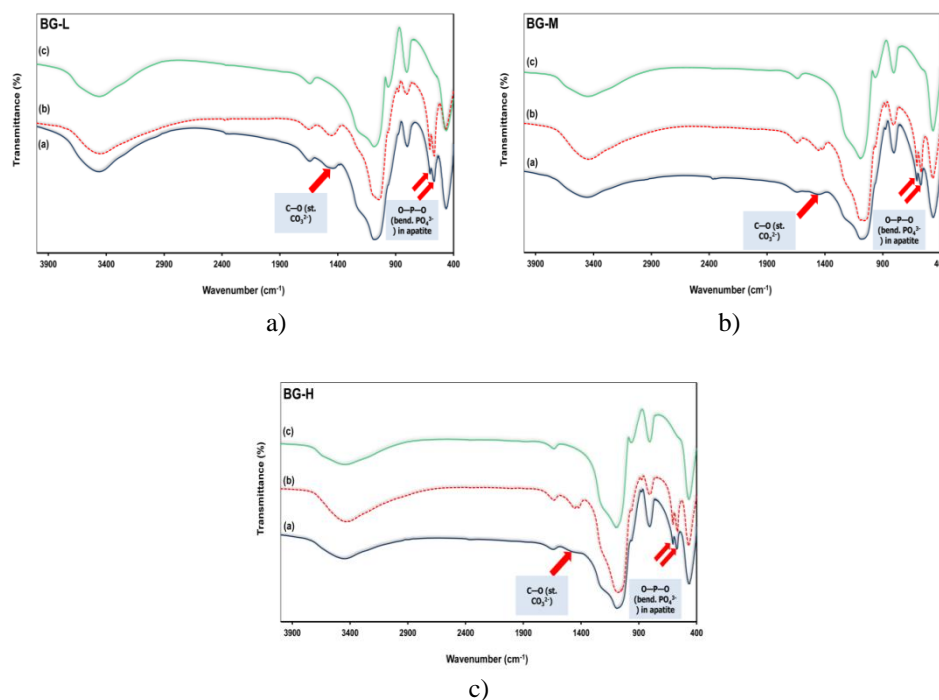


Fig. 5. FTIR spectra of BG-L, BG-M and BG-H bioactive glass powders after soaking in SBF for (a) 1 day and (b) 14 days and (c) citric acid for 14 days

In samples BG-M and BG-H after immersion in the SBF for 1 and 14 days, it can be observed that with increase of immersion time from 1 to 14 days, the peak centered at 1460 cm^{-1} gradually gets sharper and even splits into two peaks. This can be attributed to the formation of bioactive carbonated apatite layer on the surface of the glasses (the reaction between CO_2 and calcium ions into the environment or powder).

The intensity of the absorption bands at 464 and 803 cm^{-1} relating to Si-O-Si (bending) and Si-O (bending) groups decreases during immersion time from 1 day to 14 days. In contrast, the intensity of the peak at $570\text{--}602\text{ cm}^{-1}$ assigned to phosphate groups increases upon increase of immersion time showing the formation of silica gel structures and subsequently the apatite structure over time. Evolution of the peak at 960 cm^{-1} related to P-O group after 14 days of immersion in the SBF represents the breakdown of non-bridge oxygen bonds due to release of Ca ions and the dissolution of the silica in the intersection of bioglass with the SBF and also formation of P-O bonds.

It can be noted that the ratio of $\nu_4(\text{Si-O})/\nu_4(\text{P-O})$, and $\nu_1(\text{Si-O})/\nu_1(\text{P-O})$ decreases upon increase of immersion time from 1 day to 14 days. This means that in the early days of immersion the silica-rich layer is formed and subsequently the apatite layer is created. In addition, BG-L sample shows the highest Si-O/P-O ratio after 14 days of immersion in SBF. This suggests that the amount of bioactive apatite layer on surface of BG-L is lower than BG-M and BG-H, and BG-M also shows more bioactive apatite layer on its surface compared to BG-H. In general, given the higher electronegativity of Ca-O compared P-O and Si-O, Ca ions tend to break P-O and Si-O bonds and more Ca-O is formed.

In case of immersion in citric acid solution, it can be said that upon increase of Ca/P ratio in bioactive glass, the intensity of the peak at 803 cm^{-1} related to tetrahedral Si-O-Si increases meaning that more Si-O-Si is formed. With regard to the stability of orthosilicate acids in a wide range of pH, the peak at 803 cm^{-1} is likely related to the Si-O-Si groups in silicic acid. The intensity of Si-O-Si groups in citric acid is more than the SBF that is an indication of the presence of silanol groups (i.e., $\text{Si}(\text{OH})_4$).

Fig. 6 presents the SEM micrographs of the bioactive glass powders before and after soaking in SBF for 14 days. It can be clearly observed that upon increase of soaking in SBF, the

glass particles are covered with a newly formed flake-shaped layer or cauliflower-like clusters characteristic of bioactive apatite. SEM micrographs of bioactive glass samples after immersion in SBF show that in all cases the bioactive apatite layer is formed on the surface of bioactive glasses. This can be mentioned that the formation of bioactive carbonated apatite layer is a determinant step for binding of bioactive glass to the living tissue.

In microstructural scale, it can be said that BG-L is amorphous, BG-M is spherical or regular, and BG-H sample is similar to BG-M. However, it seems that the increase of calcium content in BG samples has no inhibiting effect on the growth of apatite but causes the increase of the number of germination sites and consequently decreases of the growth rate.

Fig. 7 shows the EDS patterns obtained on the surface of BG nanoparticles after soaking in SBF for 14 days. The patterns clearly show a significant increase in peak intensity of phosphorous (P) and calcium (Ca) so that in EDS pattern of all soaked BG nanoparticles the aforementioned elements become dominant. This observation can be attributed to the formation of apatite layer on the surface of the nanoparticles. Based on EDS data, the Ca/P atomic ratio in BG-L, BG-M, and BG-H nanoparticles is calculated to be 1.46, 1.89 and 1.70 respectively.

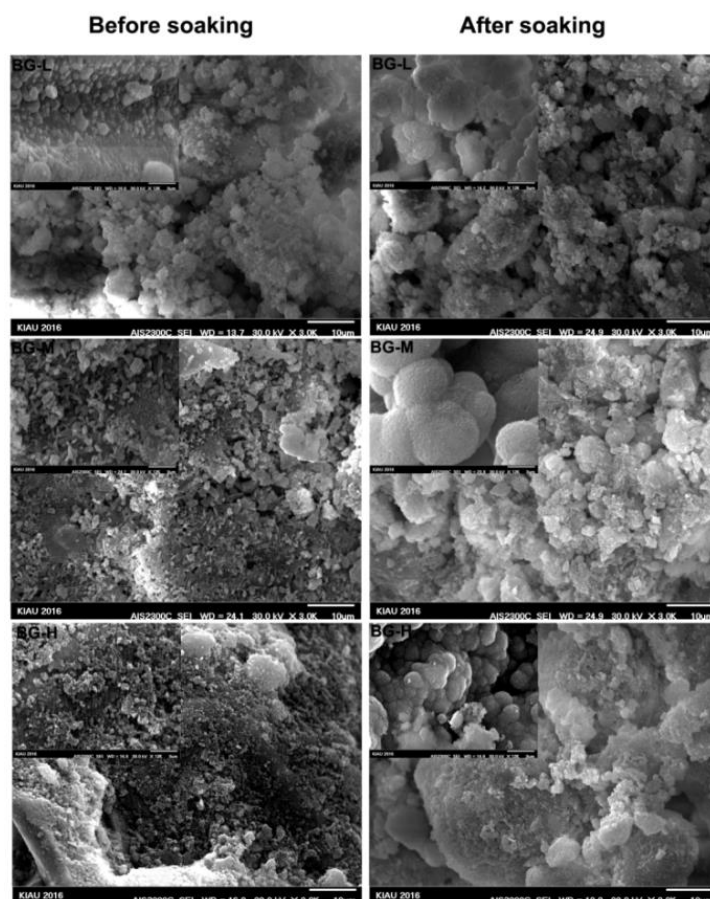


Fig. 6 SEM images of the bioactive glass powders before and after soaking in SBF solution up to 14 days

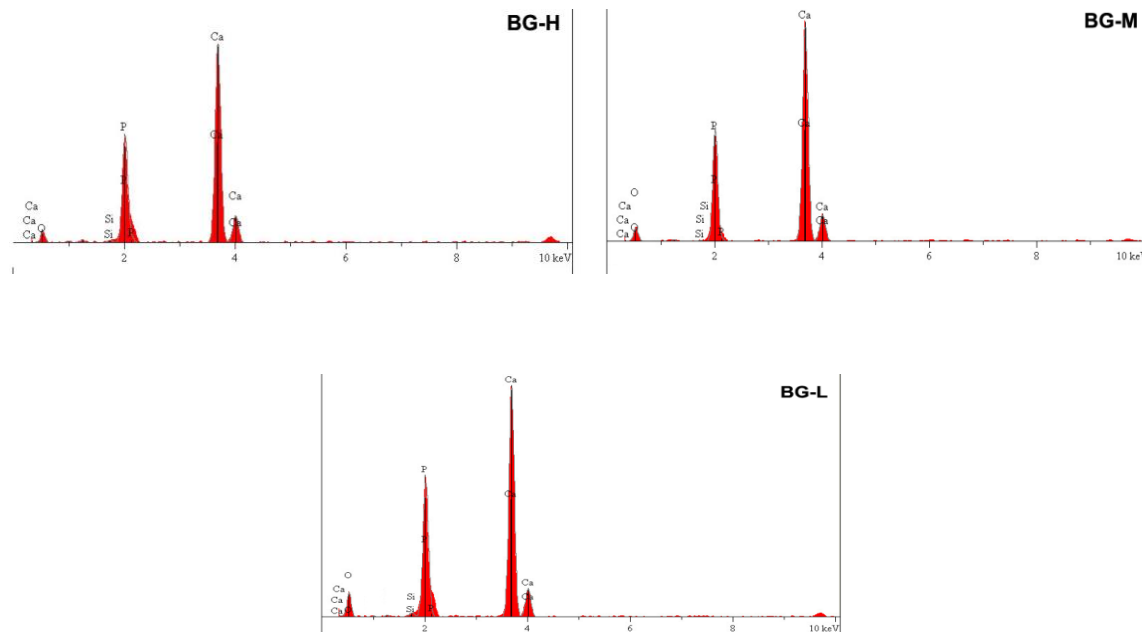


Fig. 7 EDS patterns of the soaked bioactive glass powders in SBF for 14 days

It seems that the formation of carbonated apatite layer become easier in the presence of P_2O_5 in bioactive glass, the formation of both SiO_2 and apatite rich layers on the surface of glass is promoted in the presence of NBO. Thus, the bioactivity of the glass is improved significantly by P_2O_5 and the less-polymerized Q species. Owing to increase of the less-polymerized Q^0 , Q^1 and Q^2 species, the formation of amorphous SiO_2 -rich layer on the surface of glasses with higher Ca/P ratio is facilitated. Additionally, the presence of phosphate Q species (especially $Q^0(P)-PO_4^{3-}$) in the glass is beneficial to the formation of amorphous CaO- P_2O_5 -rich layer [31,32]. A combination of two mentioned factors could be in favor of the acellular bioactivity of sample BG-M.

The Raman spectra of the synthesized BG in SBF are shown in Fig. 8. The spectra confirm the distinctive peak centered at $\sim 960\text{ cm}^{-1}$, characteristic of the symmetric stretching vibrations of the PO_4^{3-} group in the biomimetic apatite layer. There is another peak located at $\sim 1080\text{ cm}^{-1}$ assigned to the symmetric stretching vibrations of CO_3^{2-} . The emergence of the aforementioned peaks endorses the formation of carbonated apatite layer on surface of BG nanoparticles as one of the bioactivity criteria [7, 33].

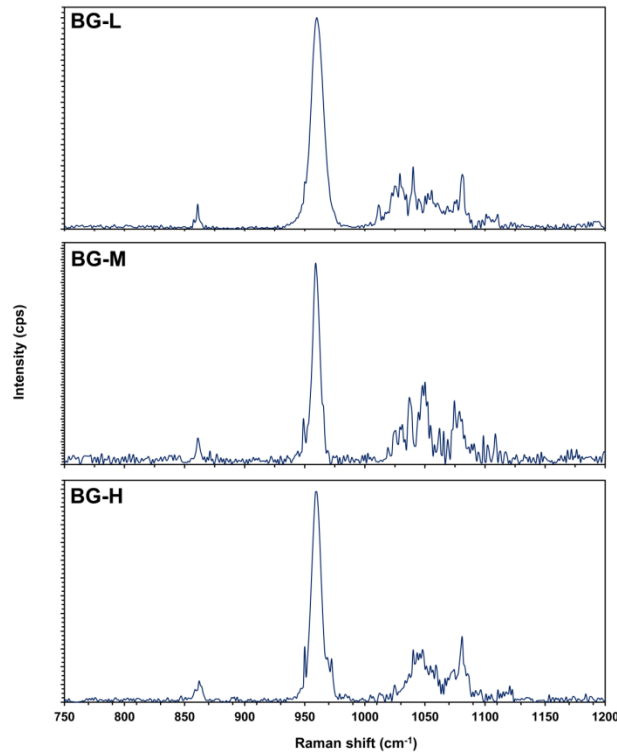


Fig. 8 Raman spectra obtained on the surface of BG powders after immersion in SBF for 14 days

Weight loss determination of the bioactive glass powders reveals the immediate degradation of the samples in the early days of immersion in SBF (Fig. 9). There is almost no difference between them in first days. The weight loss in the samples becomes stable after 7 days of immersion due to the formation of the protective apatite layer. It is clear that the bioactivity potential of the samples BG-M and BG-H, as a consequence of protective layer formation, becomes almost the same after one week.

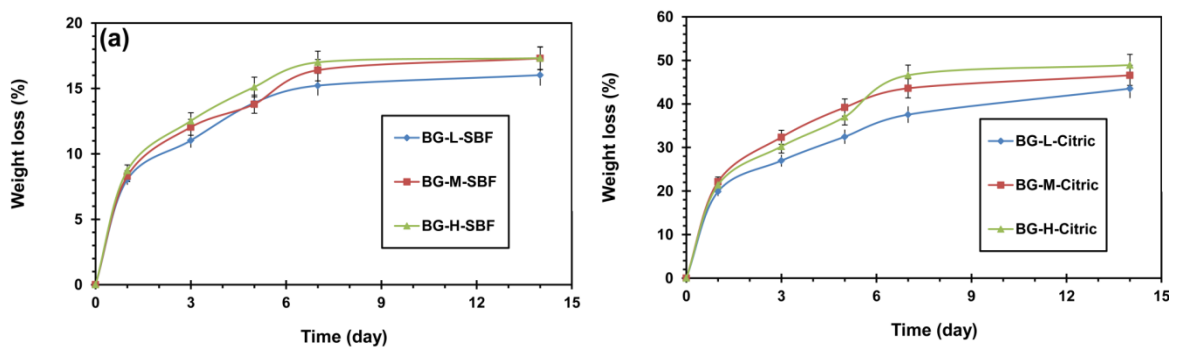


Fig. 9 The weight loss of bioactive glass powders during soaking in (a) SBF and (b) citric acid solution

In citric acid solution, a concomitant reduction in weight of the samples occurs. The weight loss measured in the first day of immersion was found to be constant for all samples. More considerable degradation found by increasing the CaO/P₂O₅ could be due to their calcium content [1, 22, 30].

Overall, bioglass samples can be arranged in terms of increasing the degradation as follows:

In SBF: BG-H≈BG-M>BG-L
 In citric acid: BG-H>BG-M>BG-L

According to the results of FTIR analysis, greater degradation of the bioglass samples in citric acid solution compared to SBF could be attributed to the lack of apatite protective layer which was discussed before.

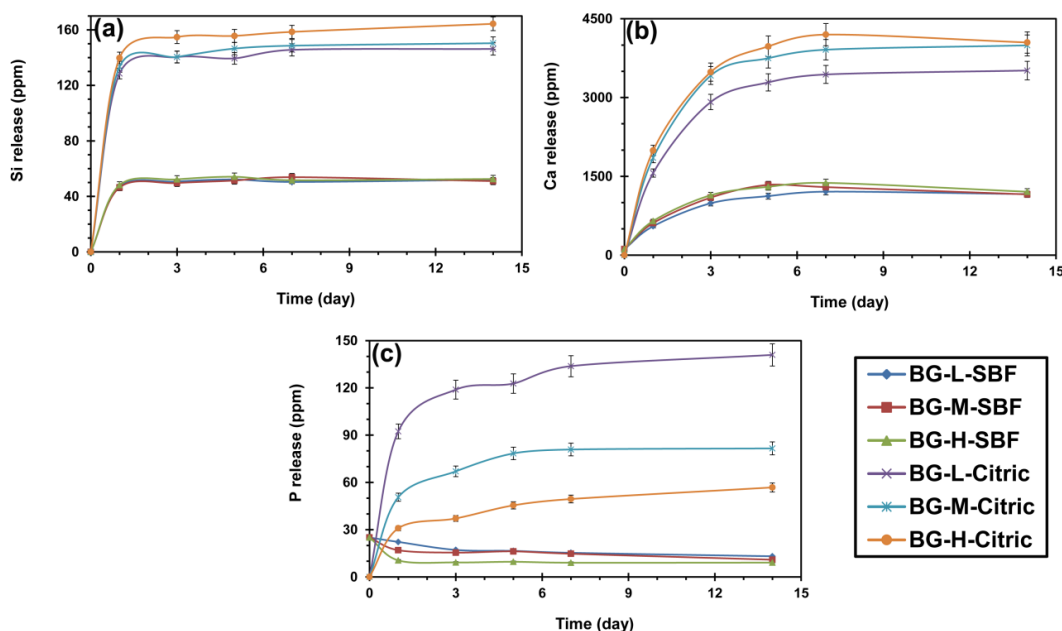


Fig. 10 The release profiles of Si, Ca, and P ions in SBF and citric acid solution

To evaluate the dissolution behavior of bioactive glass powders, the concentration of phosphorous (P), calcium (Ca) and silicon (Si) ions in the SBF and citric acid solution is measured (Fig. 10). The following results can be pointed out:

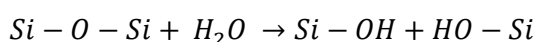
(i) As it is expected, all bioglasses show more ion release in citric acid solution compared to SBF.

(ii) During the first days of soaking, the concentrations of Ca and Si ions in SBF increase. The early depletion of phosphorus ions can be assigned to the incorporation of Ca^{2+} and PO_4^{3-} through mineralization of the newly-formed layer on the surface of the glasses [30].

In fact, the concentration of ions especially Ca^{2+} is controlled by both their release from the samples and the formation of bioactive apatite layer. Taking in to account all results from Raman and FTIR experiments as well as the concentration data until five days of immersion, it can be denounced that the release of calcium and loss of phosphorous concentration in SBF solution is further controlled by their content in the samples, whereas the protective layer plays its dominant role on the ion concentration during 3 to 5 days of immersion. In comparison with the data gathered in early days, the ICP results did not show any significant variation in long time measurement. That can be simply attributed to the fully protection of biomimetic apatite layer.

Based on the similar FTIR spectra of two weeks compared to that brought from first day of soaking, the little decrease in the concentration of both ions could be related to the formation of outer biomimetic layer.

(iii) The considerable early increase of Si^{4+} release into SBF solution can be attributed to the breaking up of outer layers of the silica glass network through the formation of Si-OH (silanols) and subsequent monosilicic acid $\text{Si}(\text{OH})_4$ at the interface of glass-solution.



The dissolution of the samples in citric acid shows a similar trend to their degradation. Actually, as it can be predicted from the FTIR results, more significant overall ion release of the bioglass samples in citric acid solution compared to SBF could be due to the lack of apatite protective layer.

Fig. 11 shows the variation of pH in SBF and citric acid solutions during the BG samples immersion. According to the figure, pH value increases during the first 7 days of immersion in SBF and then remains almost stable. The pH variations corresponds to variations in Ca^{2+} concentration because Ca^{2+} in the glass exchanged with H^+ or H_3O^+ in the SBF, and then a SiO_2 rich layer is formed on the glass surface. A similar trend occurs in citric acid solution, however because of the intensified release of alkali ions from the glass, the changes are more tangible [22, 30].

According to literature [31], the rate of hydrolysis in orthosilicates is higher than other silicate species such as disilicates and chain silicates; this means that non-bridging oxygen are more susceptible to attack compared with bridging oxygens. Therefore, the presence of orthosilicate species will facilitate the leaching of glass via H_3O^+ exchanging between solution and alkaline earth ions. Figs. 10 and 11 clearly show that increase of CaO content of the bioactive glass is accompanied by increase of calcium dissolution which is associated with an increase in solution pH.

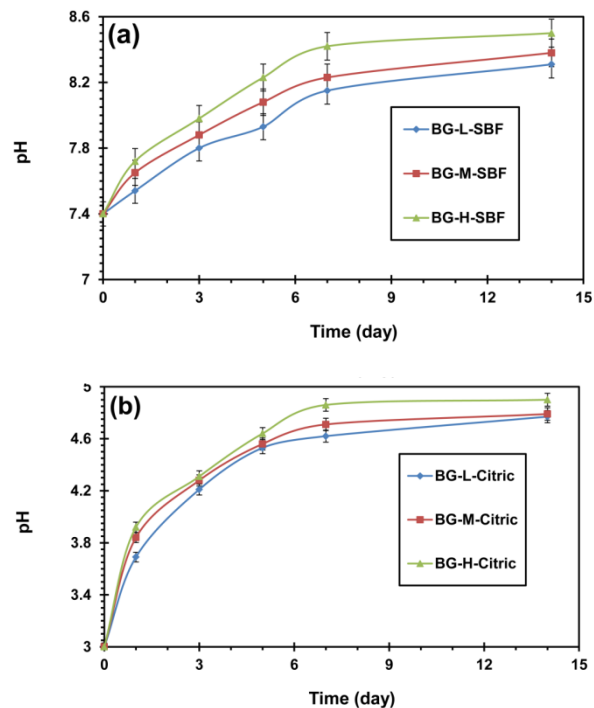


Fig. 11 pH variations in (a) SBF and (b) citric acid solutions containing BG samples

Fig. 12 shows the optical density of G-292 cells cultured on the synthesized bioactive glass nanoparticles assessed by MTT test within 7 days. The cells behaved almost the same proliferation through the first day of cell culture experiments. Different results have been found for the prolonged cell culture assay. Despite of small difference ($p > 0.05$) between optical density values of cells cultivated on both samples BG-L and BG-M and control, the sample BG-H shows unexpected cell proliferation ($p < 0.05$). This can be attributed to the considerable ion release from BG-H sample compared with BG-M and BG-L deteriorating the cell growth itinerary [34, 35].

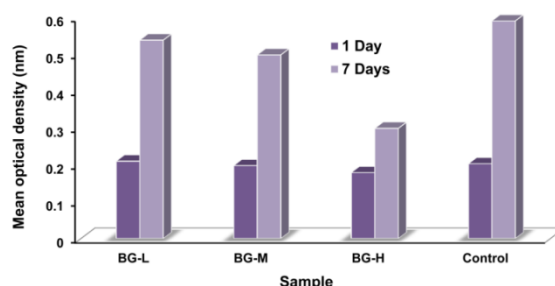


Fig. 12. The optical density of cultivated G-292 cells on bioactive glass nanoparticles

4. Conclusions

SiO₂-CaO-P₂O₅ bioactive glass nanoparticles with various CaO/P₂O₅ molar ratios of 4.75, 9.50, and 19.00 were synthesized using sol-gel method at 650 °C. The characterization results obtained from XRD, FTIR, FESEM, and EDS techniques confirmed the formation of nanoscale bioactive glass particles with high content of amorphous phase and some crystalline phases of calcium silicate. *In vitro* bioactivity study showed the rapid formation of apatite layer on the surface of the glass nanoparticles during the first days of immersion in the SBF solution. The bioactive glasses showed higher degradation in citric acid solution that were intensified upon increase of CaO/P₂O₅ ratio. In the presence of CaO, the disruption of the glass matrix network lead to formation of more non-bridging oxygens via a disproportionation reaction.

The thickness of the silica gel layer on surface of bioactive glasses could be well controlled by adjusting the CaO content of the glass. It can be deduced that the bioactivity of glasses is highly affected by glass speciation. The phosphate in the glass only helps to the nucleation of CaP phase on the surface of the glass however they are not a critical constituent due to adsorption of phosphate ions from the body fluid. MTT cytotoxicity assay suggested the non-cytotoxicity of the synthesized bioactive glass nanoparticles. Based on the obtained results, the BG-M sample is recommended as the optimum sample for further biological investigations.

References

- [1] X. F. Zhang, S. Kehoe, S.K. Adhi, T.G. Ajithkumar, S. Moane, H. O'Shea, D. Boyd, Mater. Sci. Eng. C **31**, 669 (2011).
- [2] M. Cicuéndez, M.T Portolés, I. Izquierdo-Barba, M. Vallet-Regí, Chem. Mater. **24**(6), 1100 (2012).
- [3] M.M. Stevens, Mater. Today **11**(5), 18 (2008).
- [4] J.R. Jones, Acta Biomater. **9**, 4457 (2013).
- [5] Q. Chen, G.A. Thouas, Acta Biomater. **7**, 3616 (2011).
- [6] M. Bohner, Mater. Today **13**, 24 (2010).
- [7] D. Bellucci, A. Sola, A. Anesi, R. Salvatori, L. Chiarini, V. Cannillo, Mater. Sci. Eng. C **51**, 196 (2015).
- [8] N. A. J. M. Sommerdijk, E. N. M. Van Leeuwen, M. R. J. Vosa, J. A. Jansen, Cryst. Eng. Comm. **9**, 1209 (2007).
- [9] P. Wang, L. Zhao, J. Liu, MD. Weir, X. Zhou, HH. Xu, Bone Res. **14017** (2014).
- [10] H. Oudadesse, A.C. Derrien, S. Martin, H. Chair, G. Cathelineau, Appl. Surf. Sci. **225**(2), 593 (2008).
- [11] J. Faure, R. Drevet, A. Lemelle, A. Tara, H. El Btaouri, N. Ben Jaber, H. Benhayoune, Mater. Sci. Eng. C **47**, 407 (2015).
- [12] E. Rezabeigi, P.M. Wood-Adams, R.A.L. Drew, Mater. Sci. Eng. C **40**, 248 (2014).
- [13] J. Ma, C.Z. Chen, D.G. Wang, X.G. Meng, J.Z. Shi, Ceram. Int. **36**, 1911 (2010).
- [14] A. Saboori, M. Rabiee, F. Moztarzadeh, M. Sheikhi, M. Tahriiri, M. Karimi, Mater. Sci. Eng.

- C **29**, 335 (2009).
- [15] K. Zheng, M. Lu, B. Rutkowski, X. Dai, Y. Yang, N. Taccardi, U. Stachewicz, A. Czyska-Filemonowicz, N. Hüser, A.R. Boccaccini, *J. Mater. Chem. B* **4**, 7936 (2016).
- [16] A. I. Martín, A. J. Salinas, M. Vallet-Regí, *J. Eur. Ceram. Soc.* **25**(16), 3533 (2005).
- [17] Ö.H. Andersson, I. Kangasniemi, *J. Biomed. Mater. Res.* **25**, 1019 (1991).
- [18] L.L. Hench, *J. Mater. Sci: Mater. Med.* **17**, 967 (2006).
- [19] A. Villalpando-Reyna, D.A. Cortés-Hernández, A. Gorokhovskiy, J.M. Almanza-Robles, J.C. Escobedo-Bocardo, *Ceram. Int.* **37**, 1625 (2011).
- [20] K. Huang, S. Cai, G. Xu, M. Ren, X. Wang, R. Zhang, S. Niu, H. Zhao, *Surf. Coat. Tech.* **240**, 137 (2014).
- [21] G.M. Luz, J.F. Mano, *Nanotechnology* **22**, 494014 (2011).
- [22] M. Mami, A. Lucas-Girot, H. Oudadesse, R. Dorbez-Sridi, F. Mezahi, E. Dietrich, *Appl. Surf. Sci.* **254**, 7386 (2008).
- [23] C. Gao, T. Liu, C. Shuai, S. Peng, *Scientific Reports*, **4**, 4712 (2014).
- [24] M. De Barros Coelho, M. Magalhães Pereira, *J. Biomed. Mater. Res. B Appl. Biomater.* **75**, 451 (2005).
- [25] X.V. Bui, H. Oudadesse, Y.L. Gal, O. Merdrignac-Conanec, G. Cathelineau, *Korean J. Chem. Eng.* **29**(2), 215 (2012).
- [26] P. Soares, C.A.H. Laurindo, R.D. Torres, N.K. Kuromoto O., Peitl, E.D. Zanotto, *Surf. Coat. Tech.* **206**(22), 4601 (2012).
- [27] A. J. Salinas, A. I. Martín, M. Vallet-Regí, *J. Biomed. Mater. Res.* **61**, 524 (2002).
- [28] S. Padilla J., Román, A. Carenas, M. Vallet-Regí, *Biomater.* **26**(5), 475 (2005).
- [29] S. Zhao, Y. Li, D. Li, *J. Mater. Sci: Mater. Med.* **22**, 201 (2001).
- [30] M. Mozafari, F. Moztafzadeh, M. Tahriri, *J. Non-Cryst. Solids* **356**, 1470 (2010).
- [31] J.M. Oliveira, R.N. Correia, M.H. Fernandes, *Biomater.* **23**, 371 (2002).
- [32] J. Serra, P. Gonzalez, S. Liste, S. Chiussi, B. Leon, M. Perez-Amor, H.O. Ylanen, M. Hupa, *J. Mater. Sci. Mater. Med.* **13**, 1221 (2002).
- [33] M. Campillo, P.D. Lacharmoise, J.S. Reparaz, A.R. Goñi, M. Valiente, *J. Chem. Phys.* **132**, 244501 (2010).
- [34] E. A. Abou Neel, D.M. Pickup, S.P. Valappil, R.J. Newport, J.C. Knowles, *J. Mater. Chem.* **19**, 690 (2009).
- [35] A.A. Fooladi, H.M. Hosseini, F. Hafezi, F. Hosseinnejad, M.R. Nourani, *J. Biomed. Mater. Res. A* **101**, 1582 (2013).